GPS CONSTRAINTS ON AFRICA (NUBIA) AND ARABIA PLATE MOTIONS

S. McClusky(1), R. Reilinger(1), S. Mahmoud(2), D. Ben Sari(3), A. Tealeb(2)

(1) Department of Earth, Atmospheric, and Planetary Sciences, MIT, Cambridge, MA, USA.

(2) NRIAG, Helwan, Cairo, Egypt.

(3) Ecole Mohamedia d'Ingenieurs, Rabat, Morocco.

Accepted... Received...; in original form...

Abbreviated Title: Africa, Arabia Plate Motions

Corresponding author:

Dr. Simon McClusky

Massachusetts Institute of Technology

DEAPS 54-610

Cambridge, MA 02142

USA

Email: simon@chandler.mit.edu

Tel: 1-617-253-7944

Fax: 1-617-253-1699

Summary

We use continuously recording GPS (CGPS) and survey-mode GPS (SGPS) observations to determine Euler vectors for relative motion of the African (Nubian), Arabian, and Eurasian plates. We present a well-constrained Eurasia-Nubia Euler vector derived from 23 IGS sites in Europe and 4 CGPS and 3 SGPS sites on the Nubian plate (-0.95 ± 4.8°N, -21.8 ± 4.3°E, 0.06± 0.005°/Myr). We see no significant (> 1 mm/yr) internal deformation of the Nubian plate. The GPS Nubian-Eurasian Euler vector differs significantly from NUVEL-1A (21.0 ± 4.2°N, -20.6 ± 0.6°E, 0.12 ± 0.015°/Myr) implying more westward motion of Africa relative to Eurasia and slower convergence in the eastern Mediterranean. The Arabia-Eurasia and Arabia-Nubia GPS Euler vectors are less well determined, based on only 1 CGPS and 3 SGPS sites on the Arabian plate. The preliminary Arabia-Eurasia and Arabia-Nubia Euler vectors are 27.4 ± 1.0°N, 18.4± 2.5°E, 0.40 ± 0.04°/Myr, and 30.5 ± 1.0°N, 25.7 ± 2.3°E, 0.37 ± 0.04°/Myr, respectively. The GPS Arabia-Nubia Euler vector differs significantly from NUVEL-1A (24.1 ± 1.7°N, 24.0 ± 3.5°E, 0.40 ± 0.05°/Myr), but is statistically consistent at the 95% confidence level with the revised Euler vector reported by Chu and Gordon (1998) based on a reevaluation of magnetic anomalies in the Red Sea (31.5 ± 1.2°N, 23.0 ± 2.7°E, 0.40 ± 0.05°/Myr). The motion implied in the Gulf of Aqaba and on the Dead Sea fault (DSF) by the new GPS Nubia-Arabia Euler vector (i.e., ignoring possible Sinai block motion and possible internal plate deformation) grades from pure left lateral strike-slip in the Gulf and on the southern DSF with increasing compression on the central and northern DSF with relative motion increasing from 5.6 mm/yr to 7.5 mm/yr (±1 mm/yr) from

south to north. Along the northern DSF (i.e., north of the Lebanon restraining bend) motion is partitioned between 6 ± 1 mm/yr left-lateral motion parallel to the fault trace and 4 ± 1 mm/yr fault-normal compression. Relative motions on other plate boundaries (including the Anatolian and Aegean micro-plates) derived from the GPS Euler vectors agree qualitatively with the sense of motion indicated by focal mechanisms for large crustal earthquakes (M>6). Where data are available on fault-slip rates on plate bounding faults (North Anatolian fault, East Anatolian fault, Dead Sea fault, Red Sea rift), they are generally lower than, but not significantly different from, the full plate motion estimates suggesting that the majority of relative plate motion is accommodated on these structures.

Key words: Geodynamics, Lithospheric Deformation, Plate Tectonics, Satellite Geodesy

Introduction and Tectonic Setting

Plate 1 shows the present-day plate configuration in the zone of interaction of the African, Arabian, and Eurasian plates. The early (pre-Miocene) history of the Mediterranean and Middle East region is very complex, involving a number of phases of collision, basin formation, and accretion of island arcs and continental fragments (e.g., Dercourt et al., 1986; Dewey et al., 1989). The region underwent a major change during the late Oligocene (~35 Ma) when the prior dominance of northward subduction of the Neo-Tethys was replaced by the first stages of continental collision and the development of the Alpine fold and thrust belt, although earlier collision occurred in the Eocene (~60 Ma) along the Alps in association with the Apulia promontory (Italy/Adriatic). Plate reconstructions indicate that rifting of the Red Sea and separation of the African and Arabian plates was well established by the early Miocene (about 25 Ma) (e.g., Dercourt et al., 1986; Joff and Garfunkel, 1987; Steckler et al., 1988). The present-day plate configuration was initiated during the middle Miocene (~15 Ma) with initiation of left-lateral motion along the Gulf of Aqaba and DSF (e.g., Quennell, 1984; Hempton, 1987, Lyberis, 1988; Steckler et al., 1998), the principal structures accommodating relative motion between the Nubian and Arabian plates. However, a simple geometric connection between the Red Sea rift and DSF is complicated by possible motion of the Sinai block, presumably along the Gulf of Suez (e.g., Steckler et al., 1998), and possible internal deformation of the Arabian plate, most notably in the Palmyride fold and thrust belt (Chaimov et al., 1990).

During the Middle to Late Miocene (~10 Ma), the Neo-Tethys closed between Arabia and Eurasia along the Bitlis suture in SE Turkey and the Bitlis-Zagros fold and thrust belt in Iran initiating active continental collision (e.g., Sengor et al., 1985). Active deformation and associated crustal uplift in eastern Turkey, and shortening and mountain building in the Caucasus and Zagros have been attributed to this on-going continental collision (e.g., Sengor et al., 1985; Philip et al., 1989). Around 5 Ma, the East and North Anatolian faults were initiated and began accommodating the westward motion of the Anatolian plate (e.g., Sengor, 1979; Westaway, 1994, Armijo et al., 1999).

The oceanic crust within the eastern Mediterranean basin is a remnant of the Neo-Tethys caught in the impending Nubia-Eurasia continental collision. It is being actively subducted along the Hellenic and Cyprus trenches, and presumably within the complexly deformed region connecting these trenches (although less well defined) (e.g., Le Pichon and Angelier, 1979; Klemper and Ben-Avraham, 1987; Papazachos and Papaioannou, 1999). Active subduction is also occurring southwest of Italy along the Calabrian trench. Migration of the Hellenic and Calabrian trenches over the subducting oceanic plate, presumably associated with foundering of the subducted lithosphere (Le Pichon and Angelier, 1979; Malinverno and Ryan, 1986; Royden, 1993; Jolivet and Faccenna, 2000, Savelli, 2002) has produced the Aegean and Tyrrhenian basins. Slab detachment and lithospheric delamination have also been proposed as influencing the character of surface deformation in the Mediterranean (e.g., Seber et al., 1996; Wortel and Spakman, 2000).

The African "plate" consists of two separate plates divided along the East African rift system, Nubia to the west and Somalia to the east. Extension across the rift, averaged over the past 3 Ma, has been estimated from analysis of rates of sea-floor spreading to vary from (0 – 6) ± 1.5 mm/yr from south to north within the African continent (Chu and Gordon, 1999).

The western Mediterranean has accommodated about 150 - 170 km of plate convergence since the Oligocene (~40 Ma). The current configuration, and geologically recent (i.e., post-early Miocene; ~20 Ma) history of the African-Eurasian boundary in the western Mediterranean is complex involving juxtaposed compression (Betic and Rif Mountains, Atlas Mountains) and extension (Alboran sea) (e.g., Dewey et al., 1989; Gomez et al., 2000). Further west in the Atlantic Ocean, the boundary is predominantly an oceanic transform fault that connects with the Mid Atlantic Ridge near the Azores. The transform is complex involving distributed deformation, compression along the eastern segment, predominantly right-lateral, strike slip along the central segment, and extension on the westernmost segment near the Azores (e.g., Udias et al., 1976; Buforn et al., 1988; Chen and Grimison, 1989).

The most recent, geologically determined plate motions in the Mediterranean region (i.e., 3 Myr) are described by Euler vectors derived from analyses of sea-floor magnetic anomalies, transform fault orientations, and global circuit closure (e.g., DeMets et al., 1990; 1994; Jestin et al., 1994; Chu and Gordon, 1998). Estimates of present-day Euler vectors have been reported from analysis of geodetic data by Larson et al (1997) and

Sella et al. (2002). Present-day plate motions have been estimated for smaller plates and blocks in the inter-plate deformation zone from seismic, and neotectonic observations, analysis of satellite images (e.g., McKenzie, 1972, Le Pichon and Angelier, 1979; Jackson and McKenzie, 1988), and from analysis of geodetic data (e.g., Robins et al., 1995; Le Pichon et al., 1995, Reilinger et al., 1997; McClusky et al., 2000).

In this paper we use GPS observations to constrain present-day relative motion between Nubia, Arabia, and Eurasia. We use the GPS-derived motions to determine relative Euler vectors for these plates and compare them to Euler vectors determined from global and regional plate motion models and prior geodetic studies. We include motions of intervening plates/blocks (i.e., Anatolia and Aegea) determined previously by McClusky et al. (2000) and present the resulting sense and rate of deformation across plate boundaries. We consider the implications of the new, instantaneous Euler vectors for the rigidity of continental lithosphere, and possible temporal variations in plate motions.

GPS Data Analysis and Euler Vectors

The main data used for this study were continuous GPS data (CGPS) acquired by the International GPS Service (IGS) between 1992 and 2002. To improve station coverage on the African, Arabian, Anatolian, and Aegean plates we also include five eastern Mediterranean (EMED) survey mode (SGPS) campaigns measured between 1992 and 2000 [McClusky et al., 2000]. Figure 1 shows, and Table 1 summarizes the station

velocities in a Eurasia-fixed reference frame used to constrain Africa (Nubia), Arabia, and Eurasia plate motions.

We analyze the data using the GAMIT/GLOBK software [King and Bock, 1999; Herring, 1999] in a two-step approach (e.g., Dong et al. [1998]). In the first step, we use GPS phase observations from each day to estimate station coordinates, the zenith delay of the atmosphere at each station, and orbital and Earth orientation parameters (EOP). In the second step we use the loosely constrained estimates of station coordinates, orbits, and EOP and their covariances from each day, aggregated by survey, as quasi-observations in a Kalman filter to estimate a consistent set of coordinates and velocities. We provide orbital control and tie the regional EMED measurements to an external global reference frame by including in the regional analysis data from 3–5 continuously operating IGS stations for each day. The regional quasi-observations are then combined with quasi-observations from an analysis of phase data from over 100 stations performed by the Scripps Orbital and Permanent Array Center (SOPAC) at UC San Diego (Bock et al. 1997). Before estimating velocities in the second step of our analysis, we examine the time series of position estimates to determine the appropriate weights to be applied to each group's surveys. For the velocity solution, we re-weight the quasi-observations such that the normalized long-term scatter in horizontal position for each group is unity. Finally, to account for correlated errors, we add to the assumed error in horizontal position a random walk component of 2mm/$\sqrt{}$yr (McClusky et al., 2000).

The GPS-Euler vectors determined in this study and their 1-sigma uncertainties are given in Table 2 and their locations are shown in Figures 2, and 3 along with prior results from other studies (also listed and referenced in Table 2). The residual velocities (observed minus calculated; i.e., that component of the relative velocities not accounted for by the derived Euler vectors) are also shown in these Figures. Euler vectors were estimated in a simultaneous least squares solution, using the velocity solution and its full variance covariance matrix. The vector estimates are based on 23 stations located on the Eurasian plate, 8 on the Nubian plate, and 4 on the Arabian plate (Table 1).

The Nubia-Eurasia GPS Euler vector provides a very good fit to well-constrained velocities (WRMS residuals = 0.6 mm/yr for Nubia and Eurasia) at GPS stations widely distributed around the Nubian plate (Figure 2), providing strong constraints on the Euler vector (Figure 2, and Table 2). This observation also demonstrates the coherent motion of the Nubian plate with internal deformation constrained well below 1 mm/yr (1-sigma), at least on a plate-wide basis (i.e., more local deformation that does not effect overall plate coherence cannot be ruled out).

In contrast, the Arabia-Eurasia Euler vector (and consequently the Arabia-Africa Euler vector) is derived from only 4 GPS velocities (BAHR, KIZ2, GAZI, KRCD). Furthermore, sites in SE Turkey (KRCD, KIZ2, GAZI) lie near the Bitlis suture and East Anatolian fault (EAF), the boundary between the Anatolian and Arabian plates (Figure 3). While we believe that these stations are well outside the elastic strain field (i.e., GAZI is about 90 km from the mapped surface trace of the EAF, and KIZ2 is about 150

km from the Bitlis suture), faulting is complex and we cannot completely rule out some influence from plate boundary effects.

Present-day Motion Across Plate Boundaries

As indicated in Figure 2 and Table 2, there are significant differences between the well-determined GPS Nubia-Eurasia Euler vector and that reported from the NUVEL circuit closure model. The GPS Euler vector is derived from observations spanning about 10 years while the NUVEL result is based primarily on an analysis of magnetic anomalies and transform fault orientations and is reported as a 3 Myr average. The question arises whether the GPS result represents a change in plate motions during the past few million years. Sella et al. (2002) appeal to longer-term geologic data that indicate a Miocene to present deceleration of spreading in the south Atlantic (Cante and Kent, 1992) to suggest a possible explanation for slow geodetic motion of the African plate compared to the 3 Myr NUVEL-1A result. However, DeMets et al. (1990, 1994) acknowledge the shortcomings of their model that assumes a single African plate (i.e., no allowance is made for separate Nubian and Somalian plates). Current estimates for spreading rates in the East African rift reach 6 ± 1.5 mm/yr near the northern end of the rift (Chu and Gordon, 1999). These rates are similar to Africa-Eurasia relative plate motion rates. An accurate assessment of how including Nubian and Somalian plates in the NUVEL model will effect Nubia plate motion estimates will require a complete reanalysis of the data that went into this model, an effort that is proceeding at the present time (DeMets, personal comm., 2002).

As indicated in Figure 3 and Table 2, there are significant differences between the Nubia-Arabia GPS and NUVEL Euler vectors. In contrast, the more recent Nubia-Arabia Euler vector determined by Chu and Gordon (1998) from magnetic anomalies in the Red Sea (and hence a 3 Myr average like NUVEL) agrees within confidence intervals with the GPS determination with regard to the pole location and rotation rate. Given the acknowledged limitations of the NUVEL global solution, this agreement indicates no significant change in motion of the Arabian plate with respect to Nubia during the past 3 Myr, at least at the level of detection of the current data (~1 mm/yr). On going, and expanding efforts to monitor with GPS present motions of the Arabian plate should provide tighter constraints on the GPS Nubia-Arabia Euler vector allowing more definitive conclusions about possible temporal changes in Arabia plate motion.

Relative motion derived from the GPS-Euler vectors across simplified plate boundaries (Figures 3, 4A, and 5A), and earthquake focal mechanisms for large (M> 6.0), shallow (< 50 km), historic earthquakes (Figures 4B and 5B) (Harvard catalog and others; see McClusky et al., 2000 for references) provide the opportunity to examine plate interactions. The plate boundaries we show in these figures are highly schematic, particularly those located within the continental lithosphere. Inter-plate deformation is, in at least some cases, distributed across a number of tectonic structures within the boundary zone. However, we believe the relative motions shown in Figures 3, 4A, and 5A provide improved boundary conditions for more detailed studies of plate interactions (i.e., the overall motion that must be accommodated across the plate boundary zone).

The schematic Arabia-Eurasia plate boundary corresponds to the Bitlis suture and East Anatolian fault in SE Turkey and the Main Recent fault and Bitlis-Zagros fold and thrust belt in Iran. While part of Arabia-Eurasia convergence is accommodated in the Caucasus and northern Iran, we do not include these structures in our plate model since data available for this study do not constraint the partitioning of deformation across this area. The Nubia-Arabia boundary is well determined in the Red Sea (Chu and Gordon, 1998), and along the DSF (Joffe and Garfunkel, 1987) although more detailed studies indicate local complexities (e.g., Chu and Gordon, 1998, Butler et al., 1997; Gomez et al., 2001). Similarly, the general location of the subduction/transform boundaries along the Cyprus and Hellenic trenches, and to a lesser extent, the Florence rise, are reasonably well known and are well defined by narrow bands of seismicity (at least for the Hellenic and Cyprus trenches) and well imaged down-going lithosphere (e.g., Wortel and Spakman, 2000). However, along the Cyprus trench and Florence rise, the Nubian plate interacts with the Anatolian plate and along the Hellenic trench with the Aegean plate (McKenzie, 1972, McClusky et al., 2000). Accordingly, we use the Euler vectors derived by McClusky et al. (2000) for Anatolia and Aegea to estimate orientations and rates of relative motion on these boundaries (Table 2). Various models have been proposed for the plate boundary in the central Mediterranean where seismicity is more diffuse (e.g., Savelli, 2002 and references therein). As indicated in Figure 5A (i.e., large GPS residual motions relative to Eurasia), the eastern part of the Italian Peninsula is clearly not part of the Nubian or Eurasian plates and a single boundary separating Nubia and Eurasia in the central Mediterranean is overly simplistic. Because we have little quantitative information on block motions in the Adriatic (e.g., Nocquet et al., 2001), we ignore these complications

for now and show only Nubia-Eurasia motion along a boundary south of the Italian peninsula. Moving westward, we locate the Nubia-Eurasia boundary along the Calabrian trench, ignoring possible extension within the back arc. Seismicity, and hence the location of the plate boundary (or boundaries) remains diffuse through the western Mediterranean to the straights of Gibraltar. From there, the boundary is reasonably well defined to the Mid Atlantic ridge, although it is diffuse west of Gibraltar and near the Azores.

As indicated in Figure 3, the GPS result agrees very well with the orientation of relative motion predicted by the Chu and Gordon (1998) Arabia-Nubia Euler vector along the Red Sea, and DSF. The GPS motions are smaller than the geologic result, but the difference is within the uncertainties. The GPS result implies spreading rates along the Red Sea varying from 14 ± 1 mm/yr at 15°N to 5.6 ± 1 mm/yr at 27°N. The GPS Euler vector indicates left-lateral strike slip motion along the DSF in the Gulf of Aqaba, with increasing compression towards the north. Rates of motion also increase to the north along the DSF from 5.6 ± 1 mm/yr of pure left-lateral strike slip on the southernmost DSF to 7.5 ± 1 mm/yr near the DSF – EAF junction. Along the northern DSF (i.e., north of the Lebanon restraining bend) motion is partitioned between 6 ± 1 mm/yr fault parallel and 4 ± 1 mm/yr fault normal motion. The GPS results indicate compression along the southernmost Zagros (~26° N) at 23 ± 1 mm/yr, with decreasing amplitude and an increasing component of right-lateral strike slip motion to the north (19 ± 1 mm/yr at an angle of about 30° to the main structural trend of the mountain range at 35°N), although

this motion is partitioned across other structures further north of this schematic boundary (e.g., Reilinger et al., 1997, McClusky et al., 2000; Tatar et al., 2002).

Figure 4A shows relative motions along the boundaries of the Anatolian and Aegean plates, where Anatolian and Aegean plate motions are determined from results presented by McClusky et al. (2000) (see Table 2 for Euler vectors). Along the EAF (Arabia-Anatolia) motions are predominantly left-lateral, strike slip at 9 ± 1 mm/yr. There is a component of extension, particularly along the eastern segment of the fault west of the Karliova Triple Junction. The eastern segment of the Cyprus trench is characterized by left-lateral motion with increasing tension towards the east (i.e., Gulf of Iskenderum, near the junction of the DSF, EAF), consistent with the tensional focal mechanisms around the Gulf (Figure 4B). To the west, the Cyprus and Hellenic trenches are dominated by compression with a large component of left-lateral motion along the Plino-Strabo trench. The Aegean plate is moving rapidly towards the SW relative to surrounding plates (30 ± 1 mm/yr relative to Eurasia), giving rise to extension in western Turkey (10 - 15 ± 1 mm/yr), and in the Gulf of Corinth/central Greece (~30 ± 1 mm/yr), although how "extension" is accommodated in central Greece remains enigmatic (Goldsworthy et al., 2002). The North Anatolian fault (Anatolia-Eurasia) is dominated by right-lateral strike slip (24 ± 1 mm/yr) with slight compression along the easternmost segment and extension in the Marmara Sea-N. Aegean trough. Apart from the Cyprus trench – Florence Rise where seismicity rates are low (as are relative motions), these general patterns are in good agreement with the focal mechanisms shown in Figure 4B.

In the central and western Mediterranean (Figure 5A, B) a simple Nubia-Eurasia boundary is insufficient to account for the well-determined motions of IGS stations MATE and MEDI in Italy. Clearly the Italian peninsula and Adriatic are not part of either the Eurasian or Nubian plates. In contrast, the motion of at least the southern part of Sicily (NOTO; 4.2 ± 1.2 mm/yr NW) is consistent with Nubia motion (Nubia – Eurasia motion north of NOTO is 5 ± 1 NW), suggesting that the Nubia-Eurasia boundary lies north of station NOTO and south of Sardinia (i.e., CAGL displays Eurasia motion). West of Sicily, seismicity is mostly confined to the coastal region of N. Africa. Here, the GPS relative motions indicate right-lateral, strike slip and compression across the assumed, simple boundary with total relative motion of 5 ± 1 mm/yr. This sense of relative motion is qualitatively consistent with the focal mechanism solutions (Figure 5B). In the westernmost Mediterranean (Gibraltar, Alboran Sea), relative motions become increasingly right-lateral strike slip. Station SFER in southernmost Spain shows motion more consistent with Nubia than Eurasia. In addition, focal mechanisms in northern Morocco and the Alboran Sea indicate a significant component of extension. This inconsistency between GPS relative motions and seismicity suggests that deformation is more complex than implied by the simple boundary model used in our analysis, a conclusion supported by neotectonic studies (e.g., Seber et al., 1996, Gomez et al., 2000; Gutscher et al., 2002). West of Gibraltar, Nubia-Eurasia motion becomes less compressional and more right-lateral strike slip to 17° W, increasing compression to about 24° W, and a significant component of extension to the Mid Atlantic Ridge (i.e., Azores). Relative rates of motion are roughly constant along the plate boundary in the Atlantic at about 4 - 5 ± 1 mm/yr. Although focal mechanisms are mostly confined to the

Azores along the plate boundary in the Atlantic, those that are available agree qualitatively with the GPS relative motions.

Implications for Continental Deformation

It is clear form the geodetic data presented here that deformation within the zone of interaction of the Arabia, Nubia, and Eurasia plates is complex involving intervening, smaller plates or blocks (e.g., Anatolian, Aegean, Adriadic, Alboran Sea). In some areas such as western Turkey, the Zagros of western Iran, and central Greece, deformation appears to be more spatially diffuse as indicated by dense geodetic observations, the distribution of seismic activity, active faulting, and mountain building (e.g., Jackson et al., 1995, Davies et al., 1997, Tatar et al., 2002). On the other hand, more spatially dense geodetic observations for a substantial part of the eastern Mediterranean region and the distribution of historic earthquakes are at least compatible with relatively simple models involving a small number of plates or blocks with the bulk of the deformation confined to narrow block/plate boundaries (e.g., Armijo et al., 1996, McClusky et al., 2000, Kahle et al., 2000, Nocquet et al., 2001, Meade et al., 2002). Debate continues as to whether plate/block or continuum descriptions (or some combination) represent better the behavior of active deformation within the continental lithosphere of the Mediterranean region (e.g., Thatcher, 1995, Jackson et al., 1995, Davies et al., 1997, Armijo et al., 1999, McClusky et al., 2000).

As demonstrated in this paper, it is possible to determine reference frames in which the large majority of relative site motions can be reduced to insignificance for the "interior" (i.e., away from broad active boundaries) of the Nubian, Eurasian, and Arabian plates. The geodetic result for Arabia is tentative due to limited spatial coverage, however the agreement between the geodetic and geologic (i.e., Red Sea magnetic anomalies) Euler vectors suggests that further data will only strengthen this conclusion. This alone would appear to validate the utility of a plate description of contemporary deformation. However, a further test of the utility of this approach is to compare the slip rates on plate bounding faults derived from the relative Euler vectors with those determined from near-fault geodetic studies and neotectonic evidence. Sufficient data are available to do this for the North Anatolian fault (Anatolian-Eurasia boundary), East Anatolian fault (Arabian-Anatolian boundary), and the Dead Sea fault/Red Sea rift (Arabian-Nubian plate boundary).

The GPS Anatolia-Eurasia Euler vector predicts slip rates at the location of the NAF of 24 ± 1 mm/yr. Slip rates for the NAF are reported from near field GPS studies and neotectonic studies of fault offsets and ages. Meade et al., (2002) report a rate of 25.6 ± 0.7 mm/yr based on the most recent GPS data around the western segment of the NAF fault. This agreement indicates that all relative plate motion, within the measurement uncertainty, is accommodated along the fault, at least along the segment where sufficiently dense GPS data allow a local determination.

McClusky et al. (2000) review geologic evidence for NAF slip rates based primarily on total offset and age of the fault. These estimates vary widely (16 – 25 mm/yr) and are not particularly useful at this stage for comparing to predicted rates from plate motion models.

The Anatolian – Arabian Euler vector predicts 9 ± 1 mm/yr left-lateral motion on the EAF. At present, insufficient geodetic data are available in the near field of the EAF to constrain fault characteristics (slip rates and locking depths). Geologic estimates have been reported in the range 4 – 7 mm/yr (e.g., Arpat and Saroglu, 1972, Dewey et al., 1986), somewhat smaller than the plate motion estimate. This apparent discrepancy may reflect off-fault deformation, a possibility supported by neotectonic studies (e.g., Westaway, 1994). However, the significance of this apparent difference remains uncertain given the difficulty of dating fault offsets, and possible missed offsets on parallel structures.

The Nubia-Arabia GPS Euler vector predicts 5.8 ± 1 mm/yr left-lateral slip on the southern Dead Sea fault in Israel. This rate is slightly higher than that determined by regional geodetic studies confined primarily to the western side of the fault (Pe'eri et al., 2002: 2.6 ± 1.1 mm/yr) but does not differ significantly from geomorphological studies of the DSF in Israel (Klinger et al., 2000; 4 ± 2 mm/yr since the Late Pleistocene). The possibly higher DSF rate we determine in comparison to regional GPS studies could reflect active opening of the Gulf of Suez rift estimated at ~1 mm/yr (Steckler et al., 1998), but the GPS data are not yet sufficient to justify this conclusion. As stated earlier,

there is no significant difference between rates of rifting in the Red Sea as determined from analysis of marine magnetic anomalies (i.e., localized spreading along the rift axis) and those derived from overall, present-day plate motions. Although uncertainties are high (~ 25% or more of the total slip rates) these observations provide no support for substantial off-fault, or internal plate/block deformation within the continental lithosphere of the Nubian, Eurasian, or Arabian plates.

Conclusions

We present a well-constrained Nubia-Eurasia GPS Euler vector that differs significantly from the NUVEL-1A, 3 Myr average. Because of the well known limitations in the NUVEL result, it is not yet possible to determine whether this difference is due to systematic errors or changes in plate motion rates over the past 3 Myr. We also present a preliminary Arabia-Eurasia (and Arabia-Nubia) GPS Euler vector that differs from the NUVEL-1A result, but is statistically consistent with the updated 3 Myr geologic Euler vector reported by Chu and Gordon (1998). These new GPS Euler vectors, listed in Table 2, are the principal results of this study.

We resolve no significant internal deformation of the Nubian plate as a whole. The WRMS misfit to a coherent plate motion model is 0.6 mm/yr, below the resolution of the GPS data. The Nubia-Eurasia Euler vector lies about 20° south of the NUVEL-1A result. The Nubia-Eurasia GPS Euler vector implies NW-SE convergence within the Mediterranean with a substantially larger west component of motion for Nubia along the

plate boundary zone than the NUVEL result. In addition, there is little variation in rates of motion along the boundary, ranging from 5.4 ± 1 mm/yr in the eastern Mediterranean to 4.5 ± 1 mm/yr near Gibraltar.

We use a simple plate boundary model to investigate deformation within the plate boundary zones. While this model is greatly oversimplified, it allows investigation of the total deformation that is being accommodated within these areas and as such provides overall "boundary conditions" for more detailed models. The largest relative motions across plate boundaries occur along the Hellenic trench (35 ± 1 mm/yr), within the Gulf of Corinth and central Greece (~30 ± 1 mm/yr), along the North Anatolian fault 24 ± 1 mm/yr), and along the Zagros fold and thrust belt and associated deformation zones to the northeast (19 - 23 ± 1 mm/yr). These structures also display the highest seismic energy release. Slip rates on the DSF vary from pure left-lateral strike slip along the Gulf of Aqaba and southernmost DSF segment (5.6 ± 1 mm/yr) to left-lateral transpression with 6 ± 1 mm/yr strike-slip and 4 ± 1 mm/yr compression along the northern DSF in Syria. Overall, there is good, qualitative agreement between the sense of motion indicated by the GPS Euler vectors and earthquake focal mechanisms.

Acknowledgements

We are indebted to the many individuals who established and maintained the IGS GPS stations that provided much of the data used in this study, and the SOPAC Data and Analysis Center that made these data available. We thank Chuck DeMets for providing

us a copy of his software to calculate NUVEL-1A plate motion rates, and Giovanni Sella for providing us a pre-print of his paper on plate motions. Michael Steckler and James Cochran provided helpful discussions on the geological evolution of the Red Sea region. The maps in this paper were produced using the public domain Generic Mapping Tools (GMT) software (Wessel and Smith, 1995). This research was supported in part by NSF Grants EAR-9814964, EAR-9909730, INT-0001583, and NASA grant NAG-9057.

References

Armijo, R., Meyer, B., King, G.C.P., Rigo, A., & Papanastassiou, D., 1996. Quaternary evolution of the Corinth Rift and its implications for the late Cenozoic evolution of the Aegean, *Geophys. J. Int*., 126, 11-53.

Armijo, R., Meyers, B., Hubert, A., & Barka, A., 1999. Propagation of the North Anatolian fault into the northern Aegean: Timing and kinematics, *Geology*, 27, 11-53.

Arpat, E., & Saroglu, F., 1972. The East Anatolian fault system: Thoughts on its development, *Bull. Min. Res. Explor. Inst. Turkey*, 78*,* 33-39.

Bock, Y., Behr, J., Fang, P., Dean, J., & Leigh, R., 1997. Scripps Orbit and Permanent Array Center (SOPAC) and Southern California Permanent GPS Array (PGGA), in, The Global Positioning System for the Geosciences, pp. 55-61, Nat. Acad. Press, Washington, D.C.

Buforn, E., Udias, A., & Colombas, M.A., 1988. Seismicity, source mechanisms and tectonics of the Azores-Gibraltar plate boundary, *Tectonophysics*, 152*,* 89-118.

Butler, R.W.H., Spencer, S. & Griffiths, H.M., 1997. Transcurrent fault activity on the Dead Sea Transform in Lebanon and its implications for plate tectonics and seismic hazard, *J. Geol. Soc. Lond*., 154, 757-760.

Cante, S.C., & Kent, D.V., 1992. A new geomagnetic polarity time scale for the late Cretaceous and Cenozoic, *J. Geophys. Res., 97,* 13,917-13,951.

Chaimov, T.A., Barazangi, M., Al-Saad, D., Sawaf, T., & Gebran, A., 1990. Crustal shortening in the Palmyride fold belt, Syria, and implications for movement along the Dead Sea fault system, *Tectonics, 9*, 1369-1386.

Chen, W., & Grimison, N., 1989. Earthquakes associated with diffuse zones of deformation in the oceanic lithosphere: Some examples, *Tectonophysics*, 166, 133-150.

Chu, D., & Gordon, R.G., 1998. Current plate motions across the Red Sea, *Geophys. J. Int*., 135, 313-328.

Chu, D., & Gordon, R.G., 1999. Evidence for motion between Nubia and Somalia along the Southwest Indian ridge, *Nature,* 398*,* 64-67, 1999.

Davies, R., England, P., Parsons, B., Billiris, H., Paradissis, D., & Veis, G., 1997. Geodetic strain in Greece in the interval 1892-1992, *J. Geophys. Res.,* 102, 24,571-24,588.

DeMets, C., Gordon, R., Argus, D.F., & Stein, S., 1990. Current plate motions, *Geophys. J. Int.,* 101*,* 425-478.

DeMets, C., Gordon, R., Argus, D.F., & Stein, S., 1994. Effects of recent revisions to the geomagnetic time scale on estimates of current plate motion, *Geophys. Res. Lett*., 21*,* 2191-2194.

Dercourt, J., et al., 1986. Geological evolution of the Tethys belt from the Atlantic to the Pamirs since the Lias, *Tectonophysics*, 123, 241-315.

Dewey, J.F., Hempton, M.R., Kidd, W.S.F., Saroglu, F., & Sengor, A.M.C., 1986. Shortening of continental lithosphere: The neotectonics of eastern Anatolia—A young continental collision zone, in *Collision Tectonics,* edited by M.P. Coward and A.C. Ries, *Geol. Soc. Spec. Publ*., 19*,* 3-36.

Dewey, J.F., Helman, M.L., Turco, E., Hutton, D.H.W., & Knott, S.D., 1989. (in) Coward, M.P., et al., eds., Alpine Tectonics, Geological Society [London] Special Publication 45, 265-283.

Dong, D., Herring, T.A., & King, R.W., 1998. Estimating regional deformation from a combination of space and terrestrial geodetic data, *J. Geod*., 72, 200-211.

Goldsworthy, M., Jackson, J., & Haines, J., 2002. Continuity of active fault systems in Greece, *Geophys. J. Int.,* 148, 596-618.

Gomez, F., Beauchamp, W., & Barazangi, M., 2000. Role of the Atlas Mountains (northwest Africa) within the Africa-Eurasia plate-boundary zone, *Geology,* 28, 775-778.

Gomez, F., Meghraoui, M., Darkal, A.N., Tabet, C., Khawlie, M., Khair, K., Sbeinati, R., Darawcheh, R., Khair, K. & Barazangi, M., 2001. Coseismic displacements along the Serghaya fault: An active branch of the Dead Sea fault system in Syria and Lebanon, *J. Geol. Soc. Lond.,* 158, 405-408.

Gutscher, M.-A., Malod, J., Rehault, J.-P., Contrucci, I., Klingelhoefer, F., Mendes-Victor, L., and W. Spakman, 2002. Evidence for active subduction beneath Gibraltar, *Geology,* 30, 1071-1074.

Hempton, M.R., 1987. Constraints on Arabia plate motion and extensional history of the Red Sea, *Tectonics,* 6, 687-705.

Herring, T.A., 1999. GLOBK: Global Kalman filter VLBI and GPS analysis program version 4.1, Mass. Inst. of Technol., Cambridge.

Jackson, J., & McKenzie, D., 1984. Active tectonics of the Alpine-Himalayan Belt between western Turkey and Pakistan, *Geophys. J. R. Astr. Soc*., 77, 185-246.

Jackson, J., & McKenzie, D., 1988. The relationship between plate motions and seismic moment tensors, and the rates of active deformation in the Mediterranean and Middle East. *Geophys. J. R. Astr. Soc*., 93, 45-73.

Jackson, J., Haines, J., & Holt, W., 1995. The accommodation of Arabia-Eurasia plate convergence in Iran, *J. Geophys. Res.,* 100, 15,205-15,219.

Jestin, F., Huchon, P., & Gaulier, J.M., 1994. The Somalia plate and the East Africa rift system: Present-day kinematics, *Geophys. J. Int*., 116, 637-654.

Joffe, S., & Garfunkel, Z., 1987. Plate kinematics of the circum Red Sea — a re-evaluation, *Tectonophysics*, 141, 5-22.

Jolivet, L., & Faccenna, C., 2000. Mediterranean extension and the Africa-Eurasia collision, Tectonics, 19, 1095-1106.

Kahle, H.-G., Concord, M., Peter, Y., Geiger, A., Reilinger, R., Barka, A., & Veis, G., 2000. GPS derived strain rate field within the boundary zones of the Eurasian, African, and Arabian plates, *J. Geophys. Res*., 105, 23,353-23,370.

King, R.W., & Bock, Y., 1999. Documentation for GAMIT analysis software, release 9.7, Mass. Inst. of Technol., Cambridge.

Klemper, D., & Ben-Avraham, Z., 1987. The tectonic evolution of the Cyprean arc, *Anneles Tectonica,* 1, 58-71.

Klinger, Y., Avouac, J.P., Abou Karaki, N., Dorbath, L., Bourles, D., & Reyss, J.L., 2000. Slip rate on the Dead Sea transform fault in northern Araba valley (Jordan), *Geophys. J. Int*., 142, 755-768.

Larson, K.M., Freymueller, J.T., & Philipsen, S., 1997. Global plate velocities from the Global Positioning System, *J. Geophys. Res*., 102*,* 9961-9981.

Le Pichon, X., & Angelier, J., 1979. The Hellenic arc and trench system: A key to the neotectonic evolution of the eastern Mediterranean area, *Tectonophysics,* 60, 1-42.

Le Pichon, X., Chamot-Rooke, N., Lallemant, S., Noomen, R., & Veis, G., 1995. Geodetic determination of the kinematics of central Greece with respect to Europe: Implications for eastern Mediterranean tectonics, *J. Geophys. Res*., 100*,* 12,675-12,690.

Lyberis, N., 1988. Tectonic evolution of the Gulf of Suez and the Gulf of Aqaba, *Tectonophysics*, 153, 209-220.

Malverno, A., & Ryan, W.B.F., 1986. Extension in the Tyrranean Sea and shortening in the Apennines as a result of arc migration driven by sinking of the lithosphere, *Tectonics*, 5, 227-245.

McClusky S., et al., 2000. GPS constraints on plate kinematics and dynamics in the eastern Mediterranean and Caucasus, *J. Geophys. Res*., 105, 5695-5719.

McKenzie, D.P., 1972. Active tectonics of the Mediterranean region, *Geophys. J. R. Astr. Soc*., 30, 109-185.

Meade, B.J., Hager, B.H., McClusky, S., Reilinger, R.E., Ergintav, S., Lenk, O., Barka, A., & Ozener, H., 2002. Estimates of seismic potential in the Marmara region from block models of secular deformation constrained by Global Positioning System measurements, *Bull. Seismol. Soc. Am*., 92, 208-215.

Nocquet, J.-M., Calais, E., Altamimi, Z., Sillard, P., & Boucher, C., 2001. Intraplate deformation in western Europe deduced from an analysis of the International Terrestrial Reference Frame 1997 (ITRF97) velocity field, *J. Geophys. Res*., 106, 11,239-11,257.

Papazachos, B.C., & Papaioannou, Ch.A., 1999. Lithospheric boundaries and plate motions in the Cyprus area, *Tectonophysics,* 308, 193-204.

Pe'eri, S., Wdowinski, S., Shtibelman, A., Bechor, N., Bock, Y., Nikolaidis, R., & van Domselaar, M., 2002. Current plate motion across the Dead Sea fault from three years of continuous GPS monitoring, *Geophys. Res. Lett.,* 29, DOI10.1029/2001GL013879.

Philip, H., Cisternas, A., Gvishiani, A., & Gorshkov, A., 1989. The Caucasus: An actual example of the initial stages of continental collision, *Tectonophysics*, 161, 1-21.

Quennell, A.M., 1984. The western Arabia rift system, (in) Dixon, J.E., and A.H.F. Robertson, eds., The geological evolution of the eastern Mediterranean, Geological Society [London] Special Publication, 17, 775-788.

Reilinger, R., et al., 1997. Preliminary estimates of plate convergence in the Caucasus collision zone from global positioning system measurements, *Geophys. Res. Lett*., 24*,* 1815-1818.

Robins, J.W., Dunn, P.J., Torrence, M.H., & Smith, D.E., 1995. Deformation in the eastern Mediterranean, (in) Proceedings of the First Turkish International Symposium on Deformations, vol. 2, pp. 738-745, Chamber of Surv. Eng., Ankara, Turkey.

Royden, L., 1983. The tectonic expression of slab pull at continental convergent boundaries, *Tectonics*, 12*,* 303-325.

Seber, D., Barazangi, M., Ibenbrahim, A., & Demnati, A., 1996. Geophysical evidence for lithospheric delamination beneath the Alboran Sea and Rif-Betic mountains, *Nature,* 379, 785-790.

Sella, G. F., Dixon, T.H., & Mao, A., 2002. REVEL: A model for recent plate velocities from space geodesy*, J. Geophys. Res*., 107, 10.1029/2000JB000033.

Savelli, C., 2002. Time-space distribution of magmatic activity in the western Mediterranean and peripheral orogens during the past 30 Ma (a stimulus to geodynamic considerations), *J. Geodynamics*, 34*,* 99-126.

Sengor, A.M.C., 1979. The North Anatolian transform fault: Its age, offset, and tectonic significance, *J. Geol. Soc. London,* 136*,* 269-282.

Sengor, A.M.C., Gurur, N., & Saroglu, F., 1985. Strike slip faulting and related basin formation in zones of tectonic escape: Turkey as a case study, (in) K.T. Biddle, and N. Christie-Blick (eds.), Strike slip faulting and basin formation, Spec. Publ. Econ. Paleontol. Mineral, 37, 227-264.

Steckler, M.S., Berthelot, F., Lyberis, N., & Le Pichon, X., 1988. Subsidence in the Gulf of Suez: Implications for rifting and plate kinematics, *Tectonophysics*, 153, 249-270.

Steckler, M.S., Feinstein, S., Kohn, B.P., Lavier, L.L., & Eyal, M., 1998. Pattern of mantle thinning from subsidence and heat flow measurements in the Gulf of Suez: Evidence for the rotation of the Sinai and along-strike flow from the Red Sea, *Tectonics,* 17, 903-920.

Tatar, M., Hatzfeld, D., Martinod, J., Walpersdorf, A., Ghafori-Ashtiany, M., & Chery, J., 2002. The present-day deformation of the central Zagros from GPS measurements, *Geophys. Res. Lett*., 29, 10.1029/2002GL015427.

Taymaz, T., Eyidogan, H., & Jackson, J., Source parameters of large earthquakes in the East Anatolian fault zone (Turkey), 1991. *Geophys. J. Int*., 106, 537-550.

Thatcher, W., 1995. Microplate versus continuum descriptions of active tectonic deformation, *J. Geophys. Res*., 100*,* 3885--3894.

Udias, A., Lopez Arroyo, A., & Mezcua, J., 1976. Seismotectonics of the Azores-Alboran

Wessel, P., & Smith, W.H.F., 1995. New version of the generic mapping tools released, *EOS, Trans. AGU*, 76, 329.

Westaway, R., 1994. Present-day kinematics of the Middle East and eastern Mediterranean, *J. Geophys. Res*., 99*,* 12,071-12,090.

Wortel, M.J.R., & Spakman, W., 2000. Subduction and slab detachment in the Mediterranean-Carpathian region, *Science*, 290*,* 1910-1917.

Figures and Tables

Table 1. GPS velocities in a Eurasia-fixed reference frame (as defined in this study), 1-sigma uncertainties (±), and correlation between the east and north components of velocity (RHO), used to estimate Euler vectors: * = Arabia, # = Eurasia, + = Africa. Velocities for other stations shown in the figures are also listed.

Table 2. GPS-Euler vectors and 1-sigma uncertainties (EU = Eurasia, AN = Anatolia, AE = Aegea, AR = Arabia, AF = Africa, NU = Nubia, * = New result from this study).

Plate 1. Topographic and bathymetric map of the African (Nubia-Somalia), Arabian, and SW Eurasian plates showing schematic plate boundaries used in this study. Black arrows show NUVEL-1A motion of Arabia and Nubia (AF) relative to Eurasia. Abbreviations: SG, Straits of Gibraltar; BM, Betic Mountains; RM, Rif Mountains; AM, Atlas Mountains, PM, Palmyride Mountains; CM, Caucasus Mountains; B-Z, Bitlis-Zagros fold and thrust belt; GA, Gulf of Aden.

Figure 1. GPS velocities and 95% confidence ellipses in a Eurasia fixed frame used to determine Nubia, Arabia, and Eurasia relative Euler vectors. Not all GPS sites are shown on the Eurasian plate. Selected GPS velocities within the eastern and central

Mediterranean deforming zone (Anatolian, Aegean, Adriatic "plates") are also shown. Plate boundaries are as in Plate 1.

Figure 2. Nubia-Eurasia Euler poles and 1-sigma uncertainties (see Table 2). GPS station residuals and 95% confidence ellipses are also shown. Residuals for stations on the Arabia plate are from the Arabia-Eurasia Euler vector (see Table 2 and Figure 3). Sites with names (4-character ID) were used to estimate the Euler vectors for Arabia and Nubia. Seismicity (depths < 33km) (http://www.seismology.harvard.edu), and schematic plate boundaries are also shown (plate boundaries are as in Plate 1.). The WRMS GPS velocity residuals for Nubia, Arabia, and Eurasia are 0.6 mm/yr, 0.8 mm/yr, and 0.6 mm/yr, respectively.

Figure 3. GPS (this study, in red), NUVEL-1A (black), Chu and Gordon (1998) (blue), and Sella et al. (2002) (green) Euler poles and 1-sigma uncertainties, and predicted motions along the boundary of the Arabian plate (for clarity, we do not show the Sella et al. predicted motions that differ insignificantly from those determined in this study). Motions are for Arabia relative to the adjacent plate. Residual velocities and 95% confidence ellipses for Arabia (blue) and Nubia (red) are also shown. Note close agreement in orientation of relative plate motions as determined by the Chu and Gordon (1998) 3 Myr average and those determined in this study. While the GPS relative motions are less than those determined by Chu and Gordon, the difference is not significant at the 95% confidence level. Schematic plate boundaries are as in Plate 1.

Figure 4. A) Relative motions and 95% confidence ellipses on schematic plate boundaries in the eastern Mediterranean derived from the Euler vectors determined in this study. Motions around the Arabian plate are as in Figure 3. Motions around the Aegean show Aegean motion relative to bordering plates. Motions along the boundaries of the Anatolian plate show Anatolia motion relative to bordering plates, except where it is bordered by the Aegean plate. Abbreviations: NAT, North Aegean Trough; MS, Marmara Sea; PST, Plino-Strabo Trench; FR, Florence Rise, GI, Gulf of Iskenderum. B) Earthquake focal mechanisms (lower hemisphere projection) for large (M>6), shallow (< 50 km), earthquakes (http://www.seismology.harvard.edu/CMTsearch.html).

Figure 5. A) Motions of Africa (Nubia) relative to Eurasia on schematic plate boundaries in the central, and western Mediterranean, and in the eastern Atlantic Ocean derived from the Euler vectors determined in this study. Selected GPS site velocities and 95% confidence ellipses in a Eurasia-fixed reference frame are also shown. The GPS velocities at stations MEDI and MATE indicate that the eastern part of the Italian peninsula (Adriatic) is not part of either the Eurasian or African plate. Abbreviations: SG, Straits of Gibraltar; BM, Betic Mountains; AS, Alboran Sea; RM, Rif Mountains; CT, Calabrian Trench; TB, Tyrrhenian Basin. B) Earthquake focal mechanisms (lower hemisphere projection) for large (M>6), shallow (< 50 km), earthquakes (http://www.seismology.harvard.edu/CMTsearch.html).

Table 1. GPS velocities in a Eurasia-fixed reference frame (as defined in this study), 1-sigma uncertainties (±), and correlation between the east and north components of velocity (RHO), used to estimate Euler vectors: * = Arabia, # = Eurasia, + = Africa. Velocities for other stations shown in the figures are also listed.

Long. (°E)	**Lat. (°N)**	**E (mm/yr)**	**N (mm/yr)**	**E (±)**	**N (±)**	**RHO**	**SITE**
50.60	26.20	3.72	20.79	0.83	0.82	0.001	BAHR *
40.65	37.24	-5.97	16.09	1.24	1.21	-0.029	KIZ2 *
39.80	37.84	-5.71	12.83	1.73	1.73	-0.019	KRCD *
37.57	36.90	-5.20	12.47	1.21	1.11	0.000	GAZI *
-3.95	40.44	0.59	0.26	0.74	0.73	0.000	VILL #
-4.25	40.42	0.00	-0.35	0.68	0.67	0.001	MADR #
36.75	55.69	-0.12	-0.63	0.76	0.75	0.000	ZWEN #
21.03	52.09	-0.04	0.21	0.71	0.71	-0.002	JOZE #
18.93	69.66	-1.02	0.69	0.65	0.65	-0.001	TROM #
17.07	52.27	0.26	0.21	0.75	0.75	-0.001	BOR1 #
15.49	47.06	0.68	0.29	0.64	0.64	0.000	GRAZ #
13.06	52.37	0.45	0.23	0.76	0.75	-0.001	POTS #
12.87	49.14	0.66	0.90	0.61	0.61	-0.001	WTZR #
11.92	57.39	-1.02	-0.55	0.62	0.62	0.000	ONSA #
24.39	60.21	0.23	-0.67	0.67	0.66	-0.001	METS #
104.31	52.21	-1.10	-0.46	0.79	0.78	-0.005	IRKT #
92.79	55.99	-0.86	0.04	1.02	0.99	-0.006	KSTU #
129.68	62.03	-0.77	0.37	0.89	0.88	0.000	YAKT #
58.56	56.43	-0.41	0.71	1.43	1.38	0.007	ARTU #
128.86	71.63	0.62	0.94	1.14	1.13	-0.001	TIXI #
1.48	43.56	0.15	0.92	1.06	1.05	0.000	TOUL #
11.86	78.93	0.09	-0.33	0.67	0.66	-0.001	NYAL #
7.46	46.87	0.11	0.51	0.69	0.68	-0.002	ZIMM #
6.92	43.75	0.46	0.10	0.78	0.78	-0.001	GRAS #
5.81	52.17	-0.04	0.20	0.62	0.62	-0.001	KOSG #
4.35	50.79	0.10	-0.48	0.73	0.73	-0.001	BRUS #
41.56	43.78	0.48	0.95	0.97	0.96	0.000	ZECK #
8.97	39.13	1.63	0.24	0.85	0.84	-0.003	CAGL
-9.88	-40.34	5.56	2.19	1.24	1.17	0.003	GOUG +
-15.63	27.76	-3.45	0.89	0.71	0.71	0.002	MAS1 +
31.34	29.86	-1.65	5.03	0.90	0.86	0.000	HELW +
30.88	29.51	-1.97	4.57	1.11	1.07	-0.004	MEST +
27.70	-25.88	2.21	5.25	0.52	0.50	-0.003	HART +
27.23	31.34	-2.08	4.39	1.15	1.06	0.002	MATR +
20.81	-32.38	2.17	4.37	1.12	1.08	0.004	SUTH +
9.67	0.35	-0.37	3.99	1.94	1.78	-0.003	NKLG
-6.85	33.99	-3.19	2.71	2.10	1.93	0.010	RABT
14.99	36.87	-0.87	4.14	0.94	0.93	-0.001	NOTO
11.64	44.52	3.89	1.19	0.84	0.84	-0.003	MEDI
16.70	40.64	1.67	4.31	0.64	0.63	-0.002	MATE

Table 1 (continued).

Long. (°E)	**Lat. (°N)**	**E (mm/yr)**	**N (mm/yr)**	**E (±)**	**N ±**	**RHO**	**SITE**
44.50	40.22	1.97	9.18	0.96	0.96	-0.001	NSSP
34.78	32.06	-2.43	8.10	0.92	0.91	-0.001	TELA
33.39	35.14	-7.04	3.07	0.97	0.96	-0.002	NICO
23.93	38.07	-11.08	-28.37	1.50	1.47	-0.002	DION

Table 2. GPS-Euler vectors and 1 sigma uncertainties (EU = Eurasia, AN = Anatolia, AE = Aegea, AR = Arabia, AF = Africa, NU = Nubia, * = New result from this study).

PLATES	**Lat. (°N)**	**Long (°E)**	**Rate (°/Myr)**	**Ref**
*EU-NU	-0.95 ± 4.8	-21.8 ± 4.3	0.06 ± 0.005	this study
EU-NU	-17.77 ± 9.5	-20.38 ± 3.7	0.062 ± 0.005	Sella et al. (2002)
EU-AF	21.0 ± 4.2	-20.6 ± 0.6	0.12 ± 0.015	DeMets et al. (1994)
*AR-EU	27.4 ± 1.0	18.4± 2.5	0.40 ± 0.04	this study
AR-EU	25.6 ± 2.1	19.7 ± 4.1	0.5 ± 0.1	McClusky et al. (2000)
AR-EU	24.6 ± 1.6	13.7 ± 3.9	0.5 ± 0.05	DeMets et al. (1994)
AR-EU	26.29 ± 2.1	22.82 ± 1.1	0.427 ± 0.029	Sella et al. (2002)
*AR-NU	30.5 ± 1.0	25.7 ± 2.3	0.37 ± 0.04	this study
AR-NU	31.26 ± 1.3	29.55 ± 1.8	0.400 ± 0.030	Sella et al. (2002)
AR-NU	32.59	23.70	0.418	Jestin et al. (1994)
AR-NU	31.5 ± 1.2	23.0 ± 2.7	0.40 ± 0.05	Chu and Gordon (1998)
AR-NU	32.2	24	0.376	Joffe & Garfunkel (1987)
AR-AF	24.1 ± 1.7	24.0 ± 3.5	0.40 ± 0.05	DeMets et al. (1994)
AN-EU	30.7 ± 0.8	32.6 ± 0.4	1.2 ± 0.1	McClusky et al. (2000)
AN-EU	14.6	34	0.64	Jackson & McKenzie (1984)
AN-EU	14.6	34	0.78	Taymaz et al. (1991)
AN-EU	31	35.5	0.83 ± 0.1	Westaway (1994)
AN-EU	30	34	0.44	Le Pichon et al. (1979)
AN-EU	32.73	32.03	1.72	Le Pichon et al. (1995)
AN-AR	32.9 ± 1.3	40.3 ± 1.3	0.8 ± 0.2	McClusky et al. (2000)
AN-AR	-20.6	68.9	0.34	Jackson & McKenzie (1984)
AN-AR	-3.3	61.9	0.35	Taymaz et al. (1991)
AE-AN	38.0 ± 0.5	19.6 ± 1.2	1.2 ± 0.2	McClusky et al. (2000)

Plate 1.

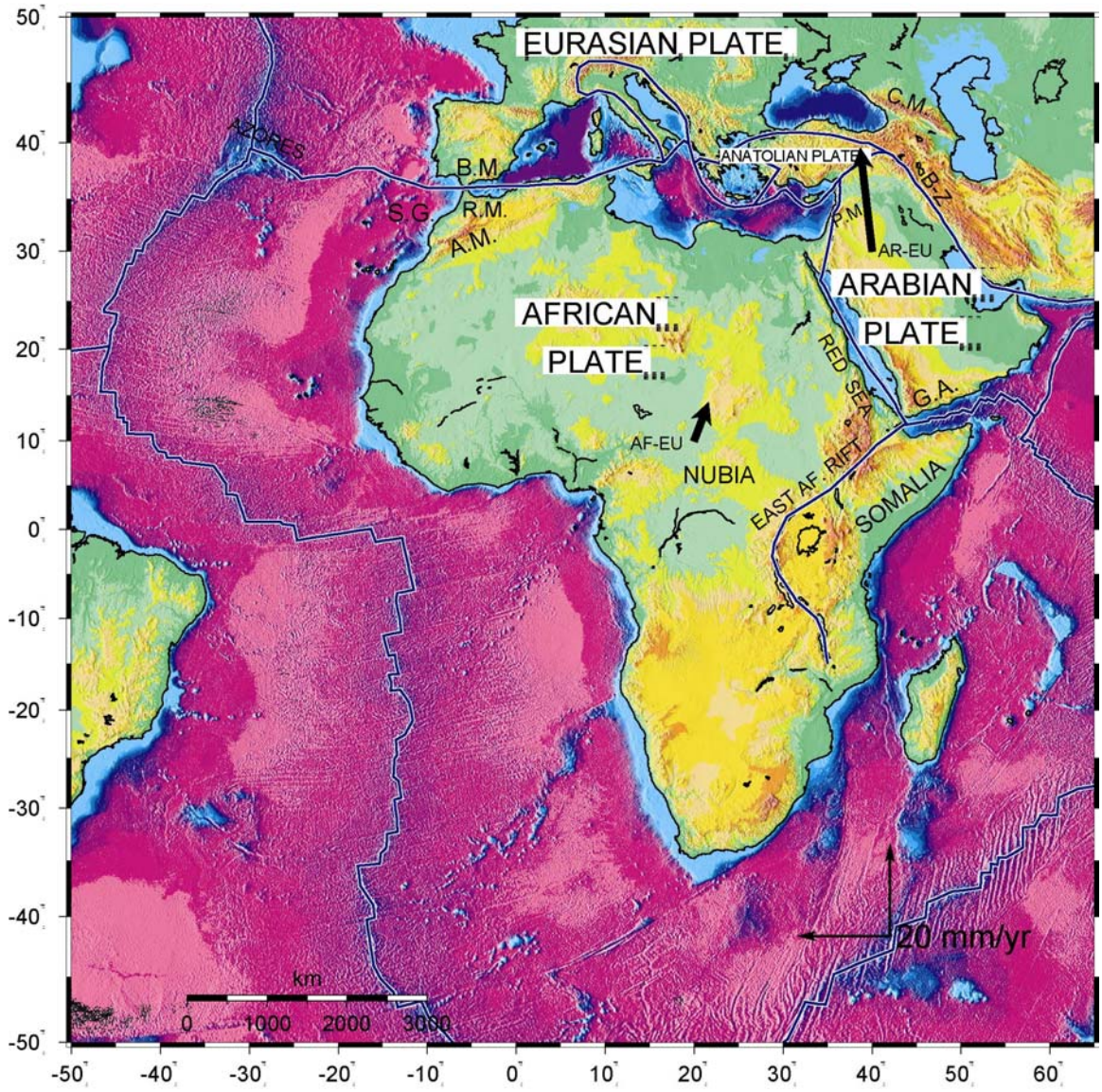
EURASIAN PLATE
AZORES
B.M.
S.G.
R.M.
A.M.
C.M.
ANATOLIAN PLATE
B.Z.
P.M.
AR-EU
ARABIAN
PLATE
AFRICAN
PLATE
RED SEA
G.A.
AF-EU
NUBIA
EAST AF. RIFT
SOMALIA
20 mm/yr
km
0
1000
2000
3000
50
40
30
20
10
0
-10
-20
-30
-40
-50
-50
-40
-30
-20
-10
0
10
20
30
40
50
60

Figure 1.

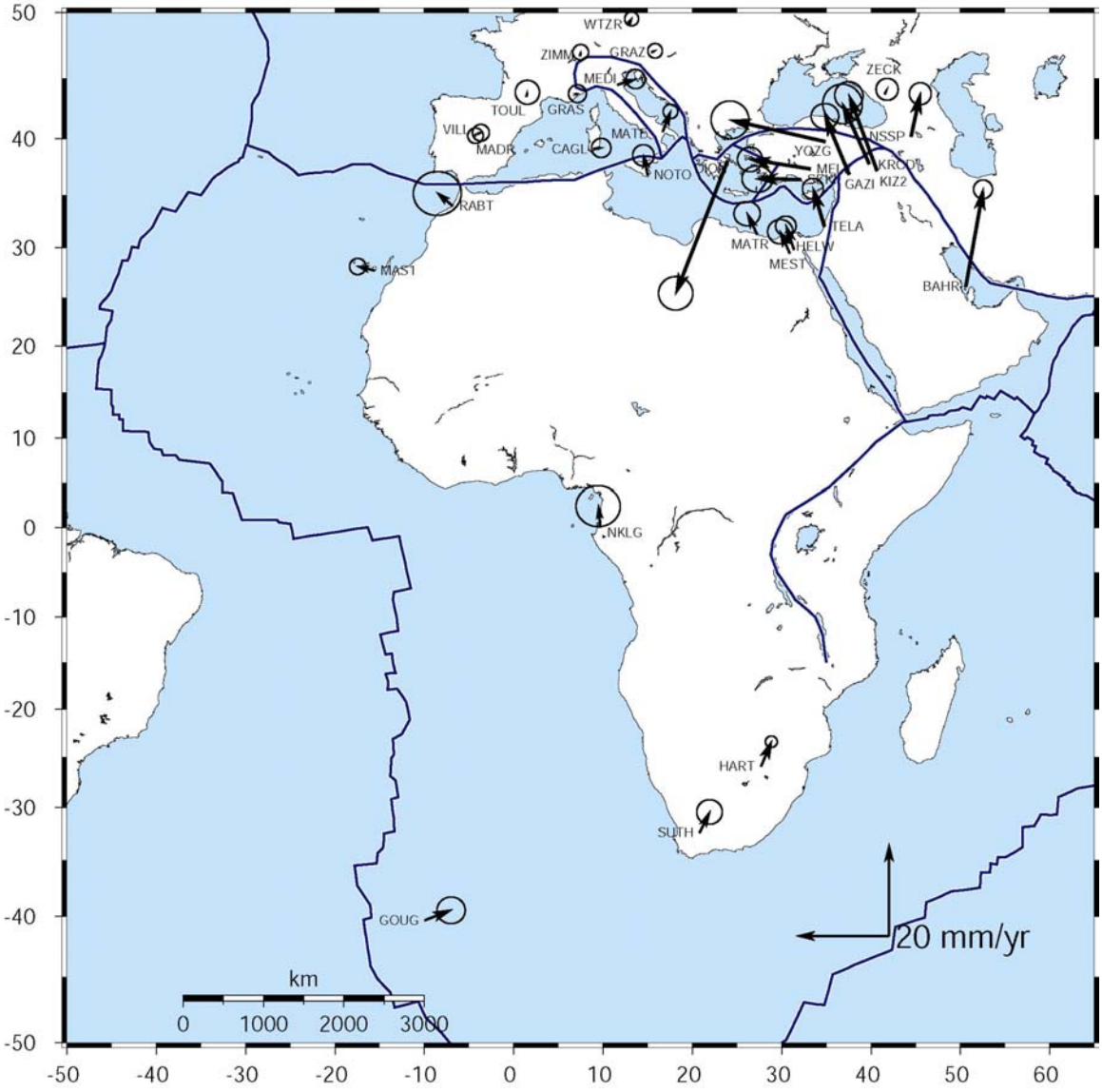
WTZR
ZIMM
GRAZ
MEDI
ZECK
TOUL
GRAS
VILL
MADR
CAGL
MATE
NOTO
YOZG
NSSP
MEL
KROO
GAZI
KIZ2
RABT
TELA
MATR
HELW
MEST
MAS1
BAHR
NKLG
HART
SUTH
GOUG
km
0
1000
2000
3000
20 mm/yr
50
40
30
20
10
0
-10
-20
-30
-40
-50
-50
-40
-30
-20
-10
0
10
20
30
40
50
60

Figure 2.

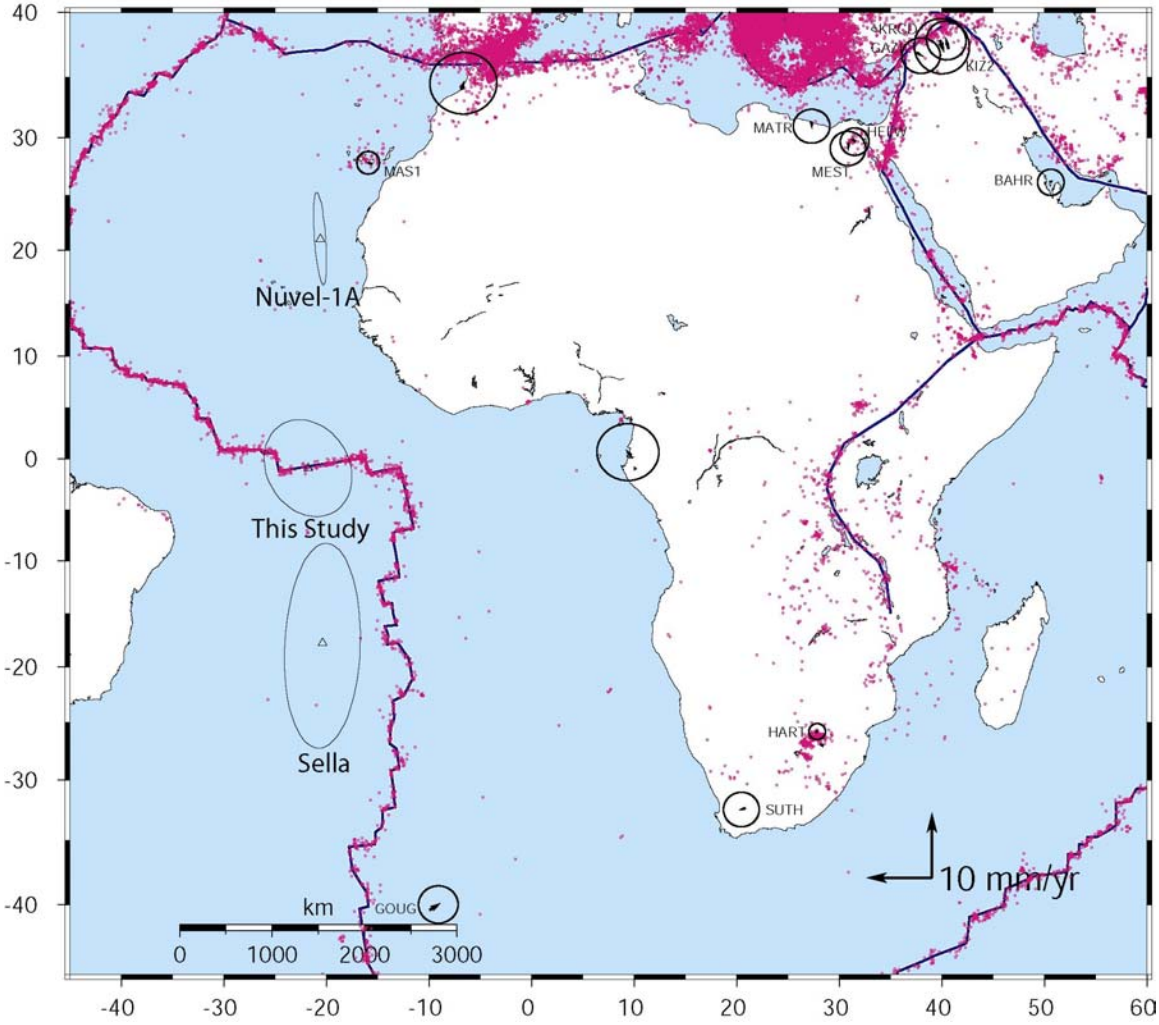
MAS1
MATR
MEST
BAHR
KIZZ
Nuvel-1A
This Study
Sella
HART
SUTH
GOUG
km
0
1000
2000
3000
10 mm/yr
40
30
20
10
0
-10
-20
-30
-40
-40
-30
-20
-10
0
10
20
30
40
50
60

Figure 3.

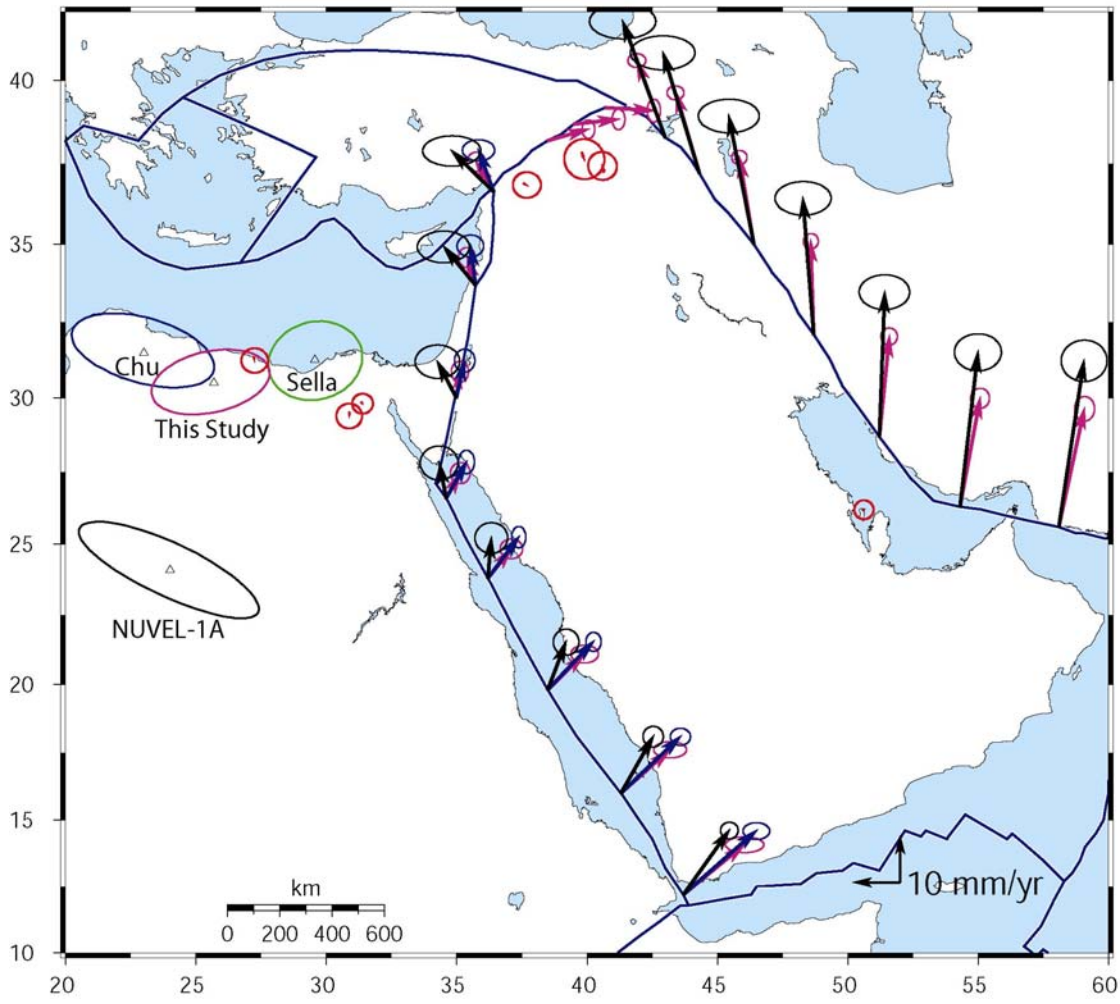
Chu
Sella
This Study
NUVEL-1A
km
0 200 400 600
10 mm/yr
40
35
30
25
20
15
10
20
25
30
35
40
45
50
55
60

Figure 4A.

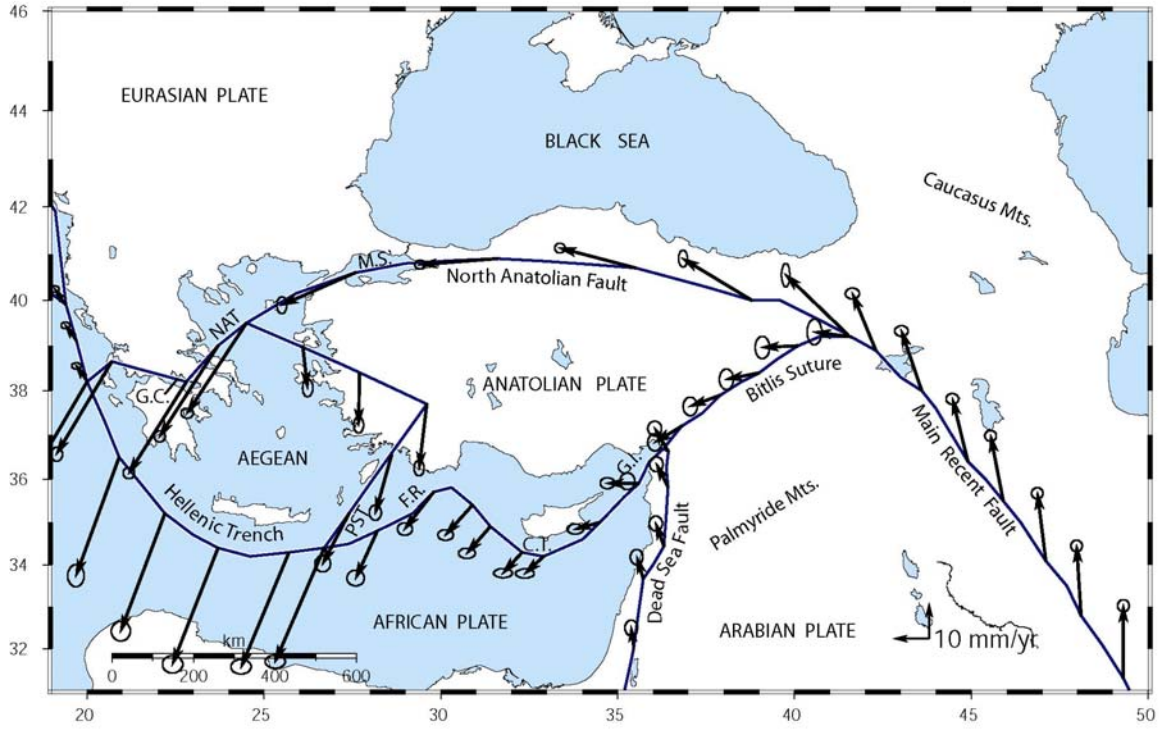

Figure 4B.

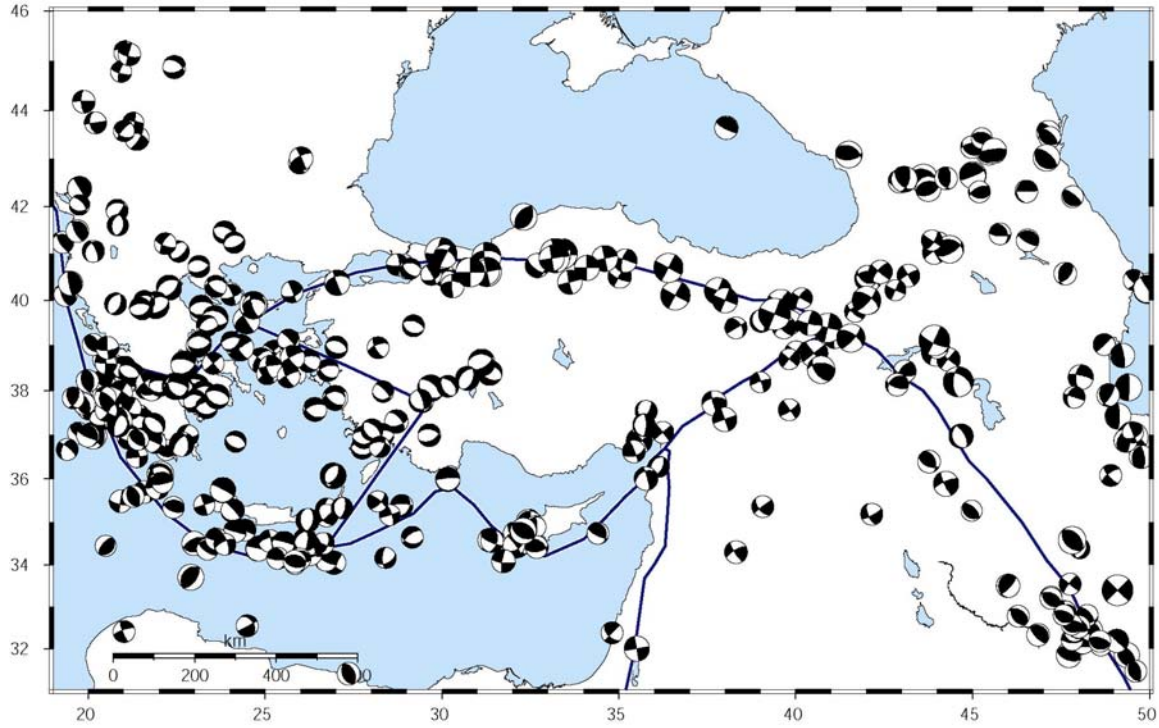

Figure 5A.

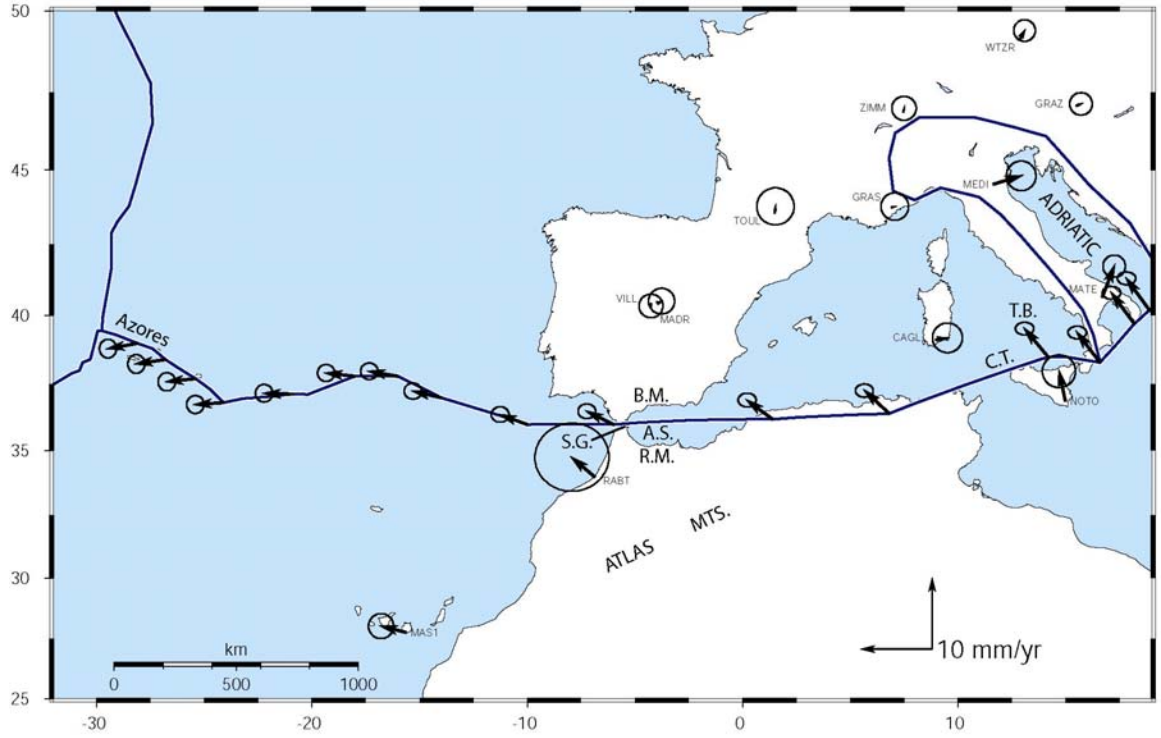

Figure 5B